Received: 22 March 2025 | Accepted: 30 September 2025

DOI: 10.1111/mice.70102

COMPUTER-AIDED CIVIL AND INFRASTRUCTURE ENGINEERING WILEY

RESEARCH ARTICLE

Machine learning-based analysis of interaction effects among influencing factors on the resilient modulus of stabilized aggregate base

Meng Guo[1,2] | **Mengmeng Zhou**[1,2] | **Xiuli Du**[1,2] | **Pengfei Liu**[3]

[1]State Key Laboratory of Bridge Engineering Safety and Resilience, Beijing University of Technology, Beijing, China

[2]The Key Laboratory of Urban Security and Disaster Engineering of Ministry of Education, Beijing University of Technology, Beijing, China

[3]Institute of Highway Engineering, RWTH Aachen University, Aachen, Germany

Correspondence

Meng Guo, State Key Laboratory of Bridge Engineering Safety and Resilience, Beijing University of Technology, Beijing 100124, China; the Key Laboratory of Urban Security and Disaster Engineering of Ministry of Education, Beijing University of Technology, Beijing 100124, China.
Email: gm@bjut.edu.cn

Pengfei Liu, Institute of Highway Engineering, RWTH Aachen University, Aachen 52074, Germany.
Email: liu@isac.rwth-aachen.de

Funding information

National Key R&D Program of China, Grant/Award Number: 2022YFE0137300; National Natural Science Foundation of China, Grant/Award Numbers: U24A20198, 52478429

Abstract

To overcome the limitations of conventional single-factor analysis, this study proposed a framework for investigating interaction effects of influencing factors on the resilient modulus (M_r) of stabilized aggregate base. First, cross-validation was utilized to compare the predictive accuracy and generalization capability of gradient boosting (GB) and random forest (RF) in predicting the M_r. The grid search algorithm was used to optimize hyperparameters. After optimization, the coefficient of determination for GB reached 0.99 on the training set and 0.96 on the test set, while those for RF were 0.98 and 0.94, respectively. The results indicated that GB demonstrated higher predictive accuracy for the M_r. Finally, the importance analysis, univariate sensitivity analysis, and bivariate interaction sensitivity analysis of influencing factors were systematically conducted using partial dependence plots (PDP) and Shapley additive explanations (SHAP). The research results showed that the importance of influencing factors on the M_r decreases in the order of maximum dry density to optimum moisture content ratio, wet–dry cycles (WDC), deviator stress, confining pressure, and ratio of oxide compounds in the cementitious materials. The bivariate interaction sensitivity analysis of the WDC, deviator stress, confining pressure, and ratio of oxide compounds in the cementitious materials did not disrupt their single-variable sensitivity relationships with the M_r. The variation of the WDC would destroy the single variable sensitivity relationship between the optimum moisture content ratio and M_r.

1 | INTRODUCTION

The structure composition of asphalt pavement is a multi-level system, which is primarily constituted by surface layer, base layer, bottom base layer, and cushion layer (P. Liu et al., 2023). Each level has its specific function and requirements. Through reasonable structural design and material selection, the performance and durability of asphalt pavement can be ensured (Swarna & Hossain, 2023). The stabilized aggregate base of asphalt pavement refers to the pavement base formed by mixing, spreading and compacting cementitious material with soil, gravel, or other aggregates (Kamran et al., 2021; Rust et al., 2022; Sharma et al., 2024). This base has good stability and

durability and is an important part of the asphalt pavement structure. For some highway sections with large traffic volume and heavy load, the use of high-quality stabilized aggregate base demonstrates remarkable enhancement in load-bearing capacity and structural longevity of the road surface.

Resilient modulus (M_r) is a key design parameter in civil infrastructure systems that quantifies the stiffness of unbound materials. M_r refers to the stress-to-strain ratio in the phase of elastic deformation of the material, which is employed for describing the capability of the material to resist elastic deformation (Alzubi et al., 2024; A. Khan et al., 2023). The M_r of stabilized aggregate base is a key index to evaluate its mechanical properties and deformation characteristics (Arulrajah et al., 2021; Ghanizadeh & Rahrovan, 2016; X. Zhang et al., 2023). The M_r of aggregate stabilized base directly influences the load-bearing capacity and resilience of the pavement. The M_r value at any site is the result of several factors that interact in multiple ways (Chowdhury, 2021; Jahanshahi & Ghanizadeh, 2025). To explore the effects stemming from different factors on the M_r of asphalt stabilized base, the researchers conducted lots of research. Wilde et al. (2016) proposed to improve the quality of aggregate base by considering the grading and shape of aggregates and finally determined an effective method with a gravel ratio of 1.4. Mizher et al. (2024) conducted unconfined compressive strength tests and monotonic triaxial tests to evaluate the interaction influence that exerts on asphalt and rubber particles on the properties of pavement base materials under certain confining pressures. The study findings revealed that the increase in the M_r caused by 3%–5% asphalt content was not enough to resist the decrease in the M_r caused by 25%-45% rubber content. Kim et al. (2014) demonstrated, with the aid of artificial neural network (ANN), that the stress state and physical properties have a significant impact on the M_r of subgrade. Hu et al. (2023) analyzed the feasibility of using foam asphalt for cold recovery cement-stabilized aggregate base by using compressive elastic modulus test, splitting strength test, and dynamic modulus test. The research results indicated that the recycled stabilized aggregate base can be used for road base construction. In the last few years, machine learning methodologies have witnessed significant advancements, providing new avenues for solving complex problems. In the domain of road engineering, researchers typically adopt laboratory testing methods to explore complex issues. However, laboratory testing methods have limitations such as long test cycles and high costs. To address these limitations, researchers have begun investigating the application of machine learning to deal with these research challenges. Ikeagwuani and Nwonu (2022) demonstrated the prediction accuracy of machine learning models by comparing their performance with that of traditional prediction models in predicting the M_r of highway base courses. Heidarabadizadeh et al. (2021) constructed a support vector machine (SVM) hybridized with the colliding bodies optimization algorithm for predicting the M_r of road materials and demonstrated the predictive accuracy of this model through model comparison. Shah et al. (2024) constructed predictive models for the M_r of pavement base using machine learning models such as SVMs, neural networks, and decision trees and employed Bayesian to achieve hyperparameter tuning for the models. The research results showed the optimized least squares boosting demonstrated the best predictive performance. K. Khan et al. (2022) developed ANN and gene expression programming (GEP) predictive models for the M_r of stabilized aggregate base. The accuracy of models was evaluated using coefficient of determination (R^2) as the performance metric, and the results demonstrated that the ANN significantly outperformed the GEP in predicting the M_r. Ikeagwuani et al. (2022) utilized the long-term pavement performance dataset to develop gradient boosting (GB), adaptive neuro-fuzzy inference system, and ANN for predicting the M_r of subgrade soils. All three machine learning methods achieved high prediction accuracy with R^2 values exceeding 0.9, demonstrating the reliability of the constructed models. Maalouf et al. (2012) used SVM to analyze the behavior of the stabilized foundation layer subjected to alternating dry and wet conditions and evaluated the influence of various factors on the M_r of stabilized aggregate base. The research results showed that SVM could accurately assess the M_r, and the dry and wet cycles had a certain influence on the M_r of stabilized aggregate base. Although some researchers have recognized the significance of machine learning in evaluating the importance and sensitivity of influencing factors for the M_r, the existing research has limitations such as low model prediction accuracy and only analyzing the sensitivity of a single factor without considering the influence patterns of the interaction between variables on the M_r.

Traditional analytical methods can only analyze the linear interactive effects between influencing factors and response indicators, whereas non-linear interactive relationships commonly exist between the M_r and the influencing factors. Forcing a linear model to fit such relationships would severely distort the actual interactions. To uncover the internal complex relationships of how different factors influence the M_r of stabilized aggregate base and to avoid the limitations of single-factor analysis, this study developed a novel framework for analyzing the interactive influence patterns of various influencing factors on the M_r of stabilized aggregate base, based on methods including GB, random forest (RF),

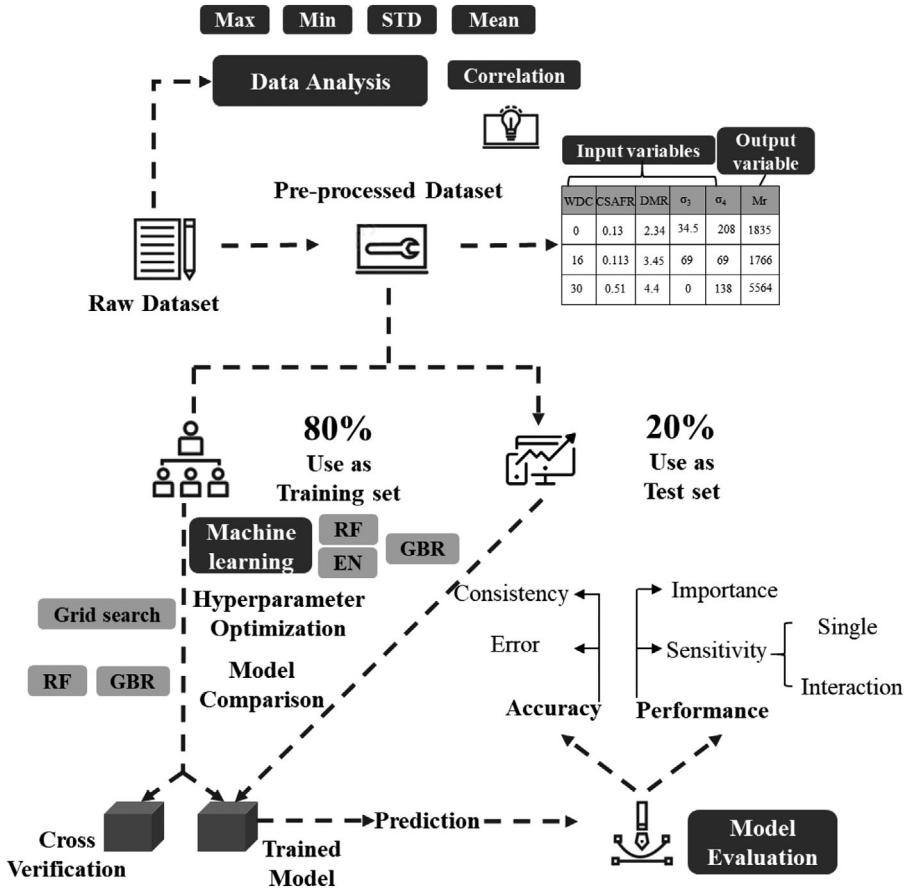

FIGURE 1 Research flow chart. RF, random forest.

cross-validation, PDP, SHAP, and so forth. First, the prediction accuracy and generalization ability of RF and GB for the M_r of stabilized aggregate base were compared through cross-validation. Then the hyperparameter of RF and GB were tuned using a grid search algorithm. Finally, based on the model with superior prediction performance, the analysis was conducted to assess the importance, individual sensitivity, and bi-variable interaction sensitivity of different influencing factors on the M_r of stabilized aggregate base. Figure 1 displays the specific research ideas.

2 | RESEARCH METHODS

2.1 | Description of the input variables

The input variables are the ratio of oxide compounds in the cementitious materials (CSAFR), wet–dry cycles (WDC), the ratio of maximum dry density to the optimum moisture content (DMR), deviator stress (σ_4) and confining pressure (σ_3), and the output variable is M_r. CSAFR directly affects the hydration reaction, influencing the cementation strength and stiffness of the material, thereby impacting the M_r of stabilized aggregate base. WDC cause repeated freezing expansion and thawing contraction of internal moisture in the material, leading to structural damage. This reduces the stiffness and performance of the material. In cold regions, WDC is one of the main influencing factors for the performance of stabilized aggregate base. The maximum dry density reflects the compactness of the material, directly affecting its strength and stiffness. The optimum moisture content refers to the water content at which maximum compaction is achieved. The DMR can comprehensively characterize the influence of compaction quality on the M_r of stabilized aggregate base. σ_4 reflects shear loading, directly influencing the stress–strain behavior of material. It can be used to simulate real-world traffic load conditions on the stabilized aggregate base. σ_3 represents the simulation of lateral confinement on the material. It can be used to model the pressure from overlying pavement layers or surrounding soil on the stabilized aggregate base. The selection of the five factors (CSAFR, WDC, DMR, σ_4, and σ_3) achieves multi-scale coverage of influencing factors from both macroscopic and microscopic perspectives. It encompasses chemical-level influences (CSAFR), pore structure-level influences (DMR), mechanical response-level influences

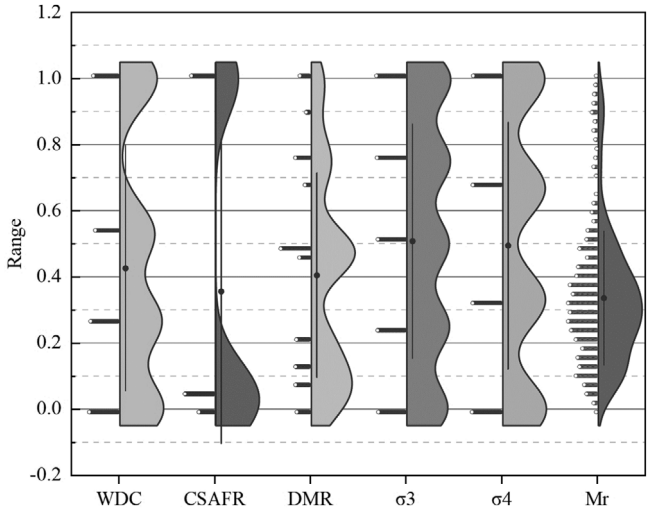

FIGURE 2 Violin diagram of variables.

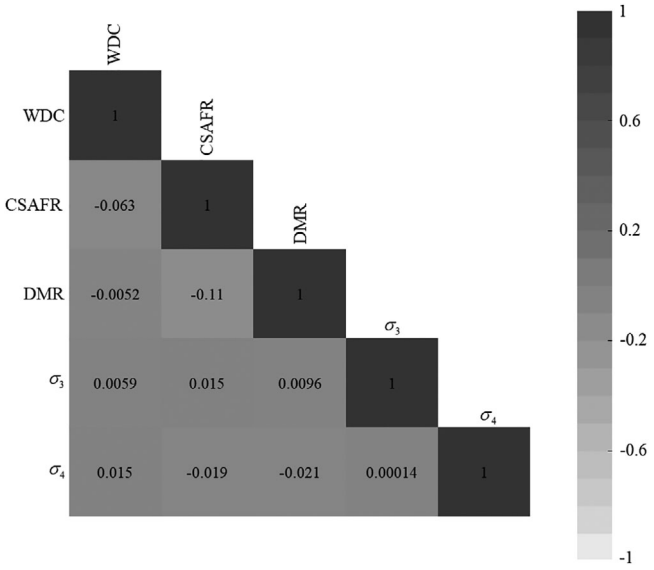

FIGURE 3 Correlation between the input variables.

(σ_4 and σ_3), and environmental effect-level influences (WDC). This effectively avoids the singularity in the selection of influencing factors for stabilized aggregate base. The 704 datasets were collected from the literature published by the Khoury research group (Khoury & Zaman, 2007; Maalouf et al., 2012). They have conducted systematic research in the field of stabilizing aggregate base for many years and published multiple research achievements. In recent years, other researchers have also carried out corresponding studies based on their experimental data, with the research findings published in authoritative journals within the field (Kaloop et al., 2019; A. Khan et al., 2023). However, the aforementioned studies did not delve into the research on how the interactive effects among influencing factors impact the M_r of stabilized aggregate base. This study primarily utilizes the experimental data from Khoury research group to analyze this research gap. Before establishing a regression prediction model, statistical analysis of datasets is an indispensable step. It helps verify the precision and reliability of the datasets and provides strong support for the construction of the model. By conducting descriptive statistical analysis, researchers can gain insights into the distribution patterns of the datasets. Violin diagram is an important way to show the distribution of data. The violin diagram of the data distribution after standardizing is displayed in Figure 2. The findings in Figure 2 show that the data distribution of WDC, DMR, σ_3, and σ_4 among the input variables is relatively uniform. To further understand the data of variables, this study analyzed the maximum, minimum, mean value, and other mathematical statistical indicators of input variables. The mathematical statistical analysis of the input variables is displayed in Table 1. As revealed in Table 1, the coverage of CSAFR, WDC, DMR, σ_3, and σ_4 is extensive, with a relatively small difference between the median and the mean, and the standard deviation is also small. These results demonstrate that the input variables have a wide coverage and a reasonable distribution, proving the reasonable of the datasets used for evaluating the M_r.

2.2 | Correlation analysis of the input variables

Correlation analysis is a quantitative technique for evaluating the magnitude and orientation of associations among variables. It helps understand whether there is a certain connection between variables and the extent of the connection. Correlation analysis can help recognize collinearity issues among input variables (Wang et al., 2023; H. Zhang et al., 2022). If there exists a high degree of correlation between input variables, it may lead to unstable estimation results of the model or produce misleading conclusions. Through correlation analysis, these problems can be found and dealt with in time to ensure the robustness of the model. Figure 3 displays the Pearson correlation analysis findings of the input variables. There exists a negative correlation between WDC and CSAFR, WDC and DMR, and the correlation coefficients are −0.063 and −0.0052, respectively. There is also a negative correlation between σ_4 and CSAFR, σ_4 and DMR, with correlation coefficients of −0.019 and −0.021, respectively. All other input variables are positively correlated. The correlation coefficients between WDC and σ_3, WDC and σ_4 are 0.0059 and 0.015, respectively. The correlation coefficient between CSAFR and σ_3 is 0.015. CSAFR and DMR have the correlational statistics of −0.11, which is the largest correlation. On the whole, the correlations between the input variables are

TABLE 1 The description statistics of the input variables.

	Wet–dry cycles (cycles)	CSAFR (%)	DMR (%kN/m^3)	σ_3 (kPa)	σ_4 (kPa)
Maximum	30.00	0.51	4.63	138.00	277.00
Minimum	0.00	0.11	2.34	0.00	69.00
Median	8.00	0.13	3.37	69.00	138.00
Mean value	12.80	0.25	3.27	70.13	171.92
Standard deviation	11.16	0.18	0.71	48.86	77.73

small. The above analysis demonstrates that the influencing factors employed in this research to analyze the M_r of the stabilized aggregate base exhibit no strong correlation with one another. Consequently, the phenomenon of multicollinearity, which undermines the accuracy of model evaluation, will be absent.

2.3 | Machine learning models

2.3.1 | RF

As a decision tree-based algorithm, RF introduces random selection attributes into the training process by leveraging Bagging technology (Bui et al., 2022; Ribeiro et al., 2023; Zhu et al., 2025). The characteristics of RF are direct principle, simple implementation, and high computational efficiency. It has shown excellent performance in small- and medium-sized datasets (hundreds of datasets; J. D. Huang et al., 2022; Qi et al., 2022; J. F. Zhang et al., 2025). The difference between RF and Bagging is that RF constructs decision trees by randomly selecting feature sets. First, establish a dataset D, $D = \{X_i, Y_i\}, X_i \in R^k, Y \in \{1, 2, 3, \ldots C\}$. Construct several decision trees randomly, and use the constructed decision trees to shape into the RF. The outcomes estimated by every single decision tree are summarized, and the ultimate prediction outputs are obtained by voting or averaging. RF improves the stability and accuracy through lowering the noise and sensitivity of the data (Xiao et al., 2024). The steps of RF construction are as follows.

1. Randomly sample n data points from the dataset (with replacement), and randomly choose k features along with the best feature node to execute splitting.
2. The newly formed collection of samples containing n data points and k features. It has a distribution of probabilities of Gini for node n, denoted as $I_{Gini}(n) = \sum_{k=1}^{K} p_k(1-p_k) = 1 - \sum_{k=1}^{K} {p_k}^2$. Classification and Regression Trees (CART) is a binary tree of $k = 2$ and is represented by $I_{Gini}(n) = 2p(1-p)$.
3. Regarding attribute A, compute $Gini(D, A)$, $Gini(D, A) = \frac{|D_1|}{|D|} Gini(D_1) + \frac{|D_2|}{|D|} Gini(D_2)$.
4. Select the best features and split nodes. Select a feature based on the principle of maximizing Gini, which will divide the values on the point into left and right offspring nodes.
5. Repeat Steps (1) to (4) to form RF.

In this study, RF was used to achieve regression prediction on the M_r of stabilized aggregate base, and grid search algorithm and cross-validation were used to achieve hyperparameter optimization and prediction accuracy verification.

2.3.2 | GB

GB is a prediction method in which a strong prediction model is constructed by combining multiple weak learners (Berangi et al., 2025; R. Huang et al., 2024). GB has demonstrated outstanding prediction results in datasets of less than a thousand groups due to its excellent performance (Y. M. Huang et al., 2023; Wu et al., 2023; Zhao et al., 2025). GB can learn models from structured datasets while maintaining high model performance, thus establishing its dominant position in the domain of predictive modeling (Khattak et al., 2023; Liang et al., 2022). In each iteration learning process, the algorithm can evaluate the deviation between the actual value and the predicted value of each sample and train a new decision tree to fit the residual with the training sample. Significantly, the research demonstrates that GB uses gradient information at each iteration to guide the construction of weak learners. Specifically, it computes the gradient of the loss function defined with respect to the parameters of the model and uses this gradient to guide the training process of the weak learners. In this way, GB can gradually optimize the performance of the model and eventually get a strong learner with good performance. Each iteration will improve the model on the basis of the results of the last iteration so as to minimize the prediction discrepancy of the model and build a model

with higher precision. The training sample set is denoted as D.

$$D = \{(x_1, y_1), (x_2, y_2), \ldots (x_m, y_m)\} \tag{1}$$

In the formula, $x_i \in X \subseteq R^n, y_i \in Y \subseteq R$, X represents the input space, Y is the output space. Suppose T represents the maximum number of iterations, $L(y, f(x))$ is the loss function, $f(x)$ is the final output of the strong learner. The GB process is as follows.

1. Initialization

$$f_0(x) = \arg\min_c \sum_{i=1}^{m} L(y_i, c) \tag{2}$$

2. Iteration

where c represents the minimum value reached by the loss function. Thus, a tree having only a root node is obtained.

Calculate the direction opposite to the gradient of the loss function for sample i, and $i = 1, 2, \ldots m$.

$$r_{t,i} = -\left[\frac{\partial L(y, f(x_i))}{\partial f(x_i)}\right]_{f(x)=f_{t-1}(x)} \tag{3}$$

where $r_{t,i}$ is the magnitude of the negative gradient in the present model, taking it as a surrogate for the residual.

For $(x_i, r_{t,i}), i = 1, 2, \ldots m$, generate a CART-based regression model. Through estimating the residual approximation, the tth regression tree is generated. Terminal node partitions of the regression tree is $R_{t,j}, j = 1, 2, \ldots J$. Calculate the best fit.

$$c_{t,j} = \arg\min_c \sum_{x_i \in R_{t,j}} L(y_i, f_{t-1}(x_i) + c) \tag{4}$$

$$f_t(x) = f_{t-1}(x) + \sum_{j=1}^{J} c_{t,j} I(x \in R_{t,j}) \tag{5}$$

In the formula, $I(x \in R_{t,j})$ represents the indicator function. If $x \in R_{t,j}$ returns 1, otherwise returns 0. Get the regression tree.

This study proposed to use the cross-validation and grid search algorithm to evaluate the prediction accuracy and optimize the hyperparameters of GB and to achieve an interpretable analysis of the association between affecting variables and the M_r of stabilized aggregate base. This study proposed to introduce PDP and SHAP into GB to realize the importance and sensitivity analysis between influencing factors and the M_r of stabilized aggregate base.

2.3.3 | K-fold cross-validation

K-fold cross-validation is a generally used technique for evaluating machine learning model, which is mainly applied to measuring the generalization ability and accuracy of the model (Jeong et al., 2022; K. Liu et al., 2022). The principle of K-fold cross-validation operationalizes by evenly randomly and evenly divides the training set into k parts, and then k-1 subsets are designated as training data to train the model, with the remaining subset reserved for validation to realize the verification of the model (Mathew et al., 2023). Finally, the original test set is applied to evaluating the effectiveness of the model in achieving its objectives again, and the results are used as the ultimate results of the model. This method makes full use of all training data, avoiding the deviation of model performance evaluation caused by improper data partitioning. Through multiple iterations and averaging, it effectively reduces the randomness of the results and improves the accuracy and generalization. K-fold cross-validation has the following advantages: (1) It reduces the performance fluctuation caused by different data splits, by training and validating multiple times. (2) Every sample is used for both training and validation, avoiding data wastage. (3) In cases of limited data, K-fold cross-validation can provide a more reliable performance evaluation.

This statistical validation technique is a simple and effective approach to assessing predictive performance that can provide more reliable performance estimates, especially for small and medium-sized datasets. With multiple training and validation, it can reduce the variance of model evaluation and help select more robust models. K = 5 represents a commonly adopted value for K in K-fold cross-validation (Fan et al., 2025; Yu et al., 2021). To enhance the accuracy of the validation results, this study additionally includes cross-validation outcomes for K = 4 and K = 6. The reliability of these two K values has also been proven (Fernandes Filho et al., 2023; Y. Liu et al., 2024; Rafie et al., 2023).

2.3.4 | Grid search algorithm

Grid search algorithm is a hyperparameter optimization method that identifies the optimal parameters configuration by exhaustively evaluating all possible combinations of hyperparameters. The principle of the grid search algorithm is to first define a list of candidate values for each hyperparameter that requires tuning, and then compute all possible combinations of these parameters. The best-performing parameters combination is ultimately selected based on the model evaluation results. Grid search algorithm has the advantages of simplicity and ease of

implementation, applicability to a wide range of models, and comprehensive coverage in hyperparameter exploration.

In this study, the grid search algorithm was employed to optimize the hyperparameters of GB and RF. For GB, the optimized hyperparameters included max_depth, subsample, learning_rate, and n_estimators. The search range for max_depth was set to (4, 10). For subsample, the candidate values were [0.5, 0.625, 0.75, 0.875, 1.0]. The search space for learning_rate included [0.05, 0.1, 0.15, 0.2, 0.25, 0.3], while n_estimators was explored across [100, 500, 1000, 1500, 2000]. For the RF, the optimized hyperparameters were max_depth and n_estimators. Specifically, the search range for max_depth was set to (4, 10), while n_estimators was explored across the candidate values [100, 500, 1000, 1500, 2000].

2.3.5 | SHAP

SHAP is a method designed to quantify the contribution of each feature to the predictive output of machine learning model, providing explanations for the decisions of the model. This method is grounded in the concept of Shapley Value from game theory, decomposing the predictions of complex black-box models into individual contribution values for each feature, thereby enabling interpretability analysis of the models. The calculation formula for the SHAP values is as follows.

$$\phi_i = \sum_{S \subseteq N \setminus \{i\}} \frac{|S|!(|N| - |S| - 1)!}{N!} (f(S \cup \{i\}) - f(S)) \quad (6)$$

In the formula, N represents the set of all features. S iterates over all subsets of features that do not contain feature i. $|N|$ denotes the total number of features. $|S|$ indicates the size of subset S. $\frac{|S|!(|N|-|S|-1)!}{N!}$ is the weight factor, accounting for the probability of subset S appearing in all possible permutations. $f(x)$ represents the predicted value. $f(S \cup \{i\}) - f(S)$ signifies the marginal contribution of feature i to subset S.

The calculation formula of SHAP values considers the marginal contribution brought by each feature when it is added to all possible combinations of features. Then, a weighting factor determined by the number of feature combinations is applied to compute the weighted average of marginal contributions. This ensures that SHAP values fairly allocate the total predictive contribution across all features. This study utilized SHAP to decompose the predictions of the M_r of stabilized aggregate base layers into feature contributions, thereby enabling interpretability analysis of the black-box predictive model.

2.3.6 | PDP

The core idea of PDP is to illustrate the marginal effect of one or two features on the predictive output of machine learning model. It reveals the relationship between features and predicted values by fixing the target feature and marginalizing the effects of other features. Its core assumption is that features are mutually independent, meaning the values of other features remain unaffected by the target feature during computation. This method is suitable for interpreting both linear and complex nonlinear relationships among features. As the model interpretability tool, PDP offers core advantages such as intuitiveness and global scope, but it also has limitations, including the masking of individual differences by averaged effects and difficulties in capturing high-dimensional interactions.

In this study, PDPs were employed to systematically demonstrate how model interpretability tools can elucidate the influence patterns of different features on the M_r of stabilized aggregate base. Additionally, the interactive effects between two features on the M_r were visualized.

2.3.7 | Optimized RF and GB

To achieve higher prediction fidelity of RF and GB on the M_r of stabilized aggregate base, this study introduced cross-validation to evaluate the accuracy and grid search algorithm to perform hyperparameter optimization of RF and GB. SHAP is a method used to explain the results generated by a machine learning model. SHAP offers a unified approach to interpreting the outputs of any machine learning model, applicable to regression, classification, and other tasks. SHAP is a powerful tool for model interpretation that aids in understanding the prediction behavior of complex models. This method is commonly applied in the fields of machine learning and data science. SHAP not only analyzes the average impact on the output magnitude but also further reveals the impact of all samples on the output. By examining the impact of each sample on the output, a clear analysis of how individual samples contribute to the output can be achieved. PDP serves as a graphical method for explaining the results made by machine learning models. It demonstrates the dependency relationship between the target variable and one or more features, while keeping other features constant. PDP aids in understanding how the model makes predictions based on specific features and is applicable to both regression and classification models. PDP is an effective model interpretation tool that helps comprehend the relationship between features and predictions, and the technique finds frequent employment across areas like data analysis and algorithmic modeling. By visualizing the marginal effect of features on predictions, PDP

provides an intuitive method for model interpretation. This study proposes the introduction of SHAP and PDP to achieve importance analysis, single-variable sensitivity analysis, and bivariate interaction sensitivity analysis of input variables on the output.

3 | RESULT AND ANALYSIS

3.1 | K-fold cross-validation results

R^2 is a core metric in statistics and predictive models used to measure the degree of agreement between the predicted results and the actual observed data. Its essence is to evaluate the ability of model to uncover data patterns or its fitting effectiveness. In this study, R^2 is used to measure the fitting effectiveness between the predicted values and the actual values. The closer R^2 is to 1, the better the fitting effectiveness. Conversely, the closer it is to 0, the worse the fitting effectiveness. Mean absolute percentage error (MAPE) is a commonly used relative error evaluation metric in predictive models, and its core function is to quantify the deviation between the predicted values and the actual values. The essence of MAPE is to calculate the arithmetic mean of the absolute percentage errors for each sample, thereby eliminating the randomness of individual sample errors and reflecting the overall relative error level of the model. A smaller MAPE indicates a smaller relative deviation between the predicted values and the actual values, implying higher prediction accuracy of the model. R^2 was selected as the prediction accuracy evaluation metric, and MAPE was selected as the prediction error evaluation metric for the models in this study. The calculation formulas for R^2 and MAPE are as follows.

$$MAPE = \frac{1}{n}\sum_{i=1}^{n}\frac{\left|y_i' - y_i\right|}{y_i} \tag{7}$$

$$R^2 = 1 - \frac{\sum_{i=1}^{n}\left(y_i - y_i'\right)^2}{\sum_{i=1}^{n}\left(y_i - \bar{y}\right)^2} \tag{8}$$

In the formula, n represents the sample size, y_i' stands for the predicted value, y_i is the actual value, and $\bar{y}$ stands for the mean of the actual values.

In this study, prediction accuracy parameters (R^2) and error parameters (MAPE) were selected to evaluate the prediction effect on the M_r of RF and GB on stabilized aggregate base.

The K-fold cross-validation (K = four, five, and six) results of RF and GB are displayed in Tables 2–4. The data in the tables show that the results of GB verification for four-fold cross-validation, five-fold cross-validation, and six-fold cross-validation are all higher than 0.97, and MAPE are lower than 0.07. The four-fold cross-validation, five-fold cross-validation, and six-fold cross-validation results of RF are all higher than 0.91, and MAPE are lower than 0.15. In cross-validation, the average R^2 values of GB are 0.974, 0.972, and 0.973 and that of RF are 0.920, 0.914, and 0.925. For mean MAPE, the average values of GB are 0.059, 0.062, and 0.058. The average values of RF are 0.137, 0.143, and 0.130. In cross-validation, GB demonstrated a higher R^2 and a lower MAPE than RF. The above analysis proves that RF and GB have excellent performance in evaluating the M_r of stabilized aggregate base, and the models have strong robustness and generalization ability. In contrast, GB has a higher prediction accuracy and stability for the M_r than RF.

3.2 | Prediction accuracy analysis

To further improve the accuracy of RF and GB in evaluating the M_r of stabilized aggregate base, this study applied the grid search algorithm to adjust the hyperparameters of RF and GB, and then used the optimized RF and GB to evaluate the M_r of stabilized aggregate base. The predictive effect of RF and GB on the M_r of stabilized aggregate base is shown in Figure 4. Model outputs for the M_r using GB align nearly perfectly with observed values in the training set, achieving an R^2 value approaching unity, with only a few scattered points deviating from the line of $R^2 = 1$. Compared to GB, RF exhibits poorer prediction performance on the training set, with a deviation between the predicted and actual values and the perfect fit curve ($R^2 = 1$). The R^2 value for RF is 0.98. In the test set, GB also demonstrates superior prediction performance for the M_r, with R^2 values of 0.96. Compared to GB, the prediction effect of RF is poorer, with R^2 values between predicted and actual values in the test set being 0.94. The aforementioned analysis demonstrates that among the optimized RF and GB, GB exhibits superior prediction accuracy for the M_r, compared to RF.

3.3 | Importance and sensitivity analysis

3.3.1 | Importance analysis

This study utilized SHAP to explain the contribution of different input variables to the M_r. Figure 5 presents the analysis results of the importance of influencing factors on the M_r. The vertical axis signifies the influencing factors, while the horizontal axis represents the mean SHAP values in Figure 5. Figure 5 indicates that the importance of the influencing factors decreases in the order of

TABLE 2 The outcomes of four-fold cross-validation.

Model	Repetition number	R^2	Mean value	Mean absolute percentage error (MAPE)	Mean value
Random forest (RF)	1	0.924	0.920	0.136	0.137
	2	0.918		0.139	
	3	0.920		0.137	
	4	0.919		0.136	
Gradient boosting (GB)	1	0.975	0.974	0.059	0.059
	2	0.972		0.060	
	3	0.974		0.058	
	4	0.975		0.059	

TABLE 3 The outcomes of five-fold cross-validation.

Model	Repetition number	R^2	Mean value	MAPE	Mean value
RF	1	0.914	0.914	0.145	0.143
	2	0.918		0.138	
	3	0.915		0.142	
	4	0.912		0.147	
	5	0.910		0.141	
GB	1	0.973	0.972	0.060	0.062
	2	0.971		0.061	
	3	0.971		0.065	
	4	0.973		0.060	
	5	0.971		0.062	

TABLE 4 The outcomes of six-fold cross-validation.

Model	Repetition number	R^2	Mean value	MAPE	Mean value
RF	1	0.926	0.925	0.132	0.130
	2	0.925		0.130	
	3	0.926		0.131	
	4	0.925		0.129	
	5	0.923		0.130	
	6	0.925		0.130	
GB	1	0.974	0.973	0.058	0.058
	2	0.973		0.059	
	3	0.973		0.059	
	4	0.974		0.057	
	5	0.973		0.059	
	6	0.973		0.059	

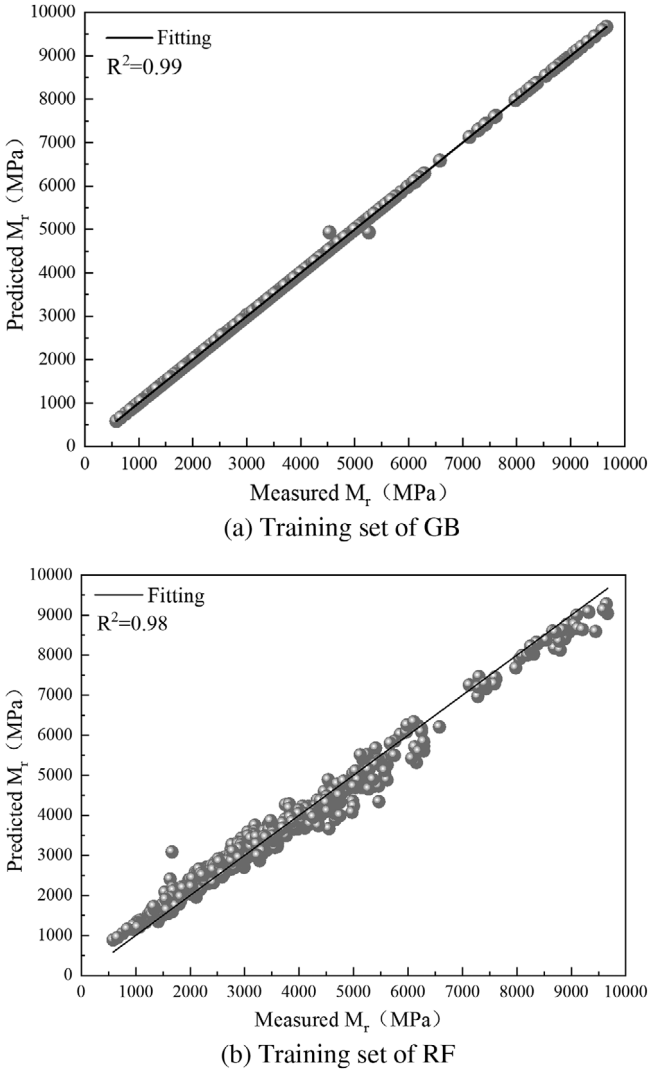

FIGURE 4 The fitting effect of the predicted and actual values. GB, gradient boosting; RF, random forest.

DMR, WDC, σ_4, σ_3 and CSAFR (A. Khan et al., 2023). DMR has the utmost importance to the M_r, significantly outpacing all other affecting variables. CSAFR has the least impact on the M_r, with its average SHAP value being roughly only one-tenth of that associated with the average SHAP value of DMR. Although the importance analysis can explore the importance of influencing factors to the M_r, it cannot be clear the change rule of the M_r with the change of influencing factors.

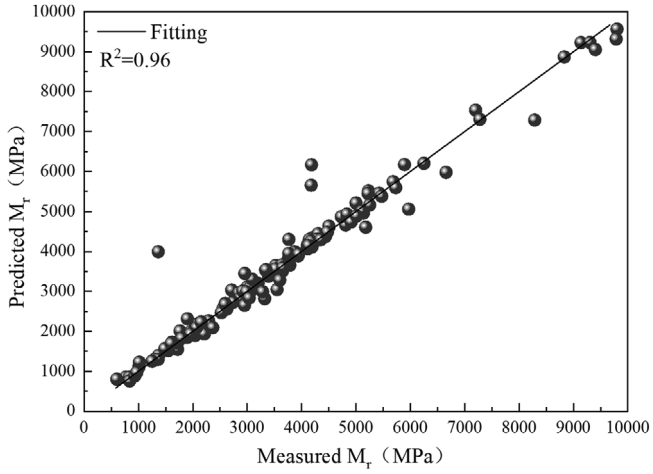

(c) Test set of GB

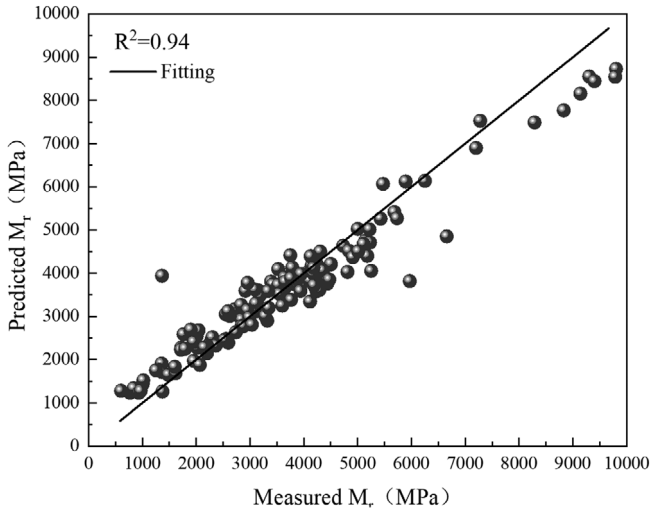

(d) Test set of RF

FIGURE 4 Continued

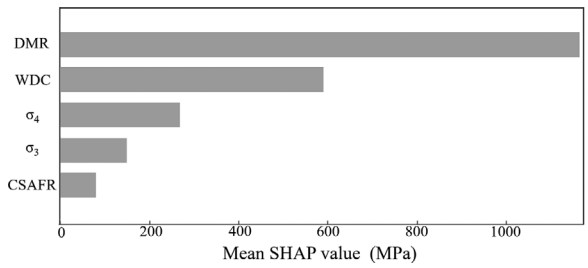

FIGURE 5 Results of importance analysis. SHAP, Shapley additive explanations.

3.3.2 | Univariate sensitivity analysis

PDP was used to further analyze the sensitivity of different input variables to the M_r. Univariate sensitivity analysis refers to the process of analyzing the individual impact of a single independent factor on the M_r while keeping other factors constant. Its physical significance lies in identifying key influencing factors, revealing the linear or nonlinear relationships between them and M_r, and providing guidance for the optimal design of stabilized aggregate base. Figure 6a shows that with the increase of DMR, M_r presents a trend of gradual increase (Heidarabadizadeh et al., 2021). When DMR is around the range of 0–2.7%kN/m^3, the increasing trend of DMR has a significant impact on the increase of the M_r. when DMR changes around the range of 2.7–4.2%kN/m^3, the positive correlation effect on the M_r is relatively small. When DMR exceeds 4.2%kN/m^3, its significant influence on the M_r reappears. The physical reasons for the above phenomenon are as follows. When the DMR is relatively small, the material exists in a relatively loose state. As the DMR increases, aggregate particles undergo reorganization during compaction, with smaller particles filling the voids between larger ones, thereby forming a denser skeletal structure. The reduction in porosity directly leads to an increase in material stiffness, resulting in a significant rise in the M_r. Figure 6b shows that WDC is significantly negatively correlated with the M_r. This is because during the dry–wet cycle, the base material may experience volume change and stress concentration, resulting in the destruction of the internal structure and the formation of micro-cracks, which will reduce the stiffness and bearing capacity of the base, thus showing a decrease in the M_r. Figure 6c indicates that as σ_4 increases, there is a gradual increase trend of the M_r (Heidarabadizadeh et al., 2021). Furthermore, when σ_4 reaches around 70 kPa, the increasing trend of the M_r becomes more significant. The information in Figure 6d suggests that the influence pattern of σ_3 on the M_r exhibits a high degree of consistency with the influence pattern of σ_4 on the M_r. Both show an increase in the M_r as the influencing factor increases, and when them reach around 70 kPa, this positive correlation becomes even more pronounced. Under low σ_4 and σ_3, aggregate particles remain loosely arranged with limited contact points between them. Constrained by interparticle friction, the M_r increases only gradually as σ_4 and σ_3 rise. However, once σ_4 and σ_3 exceed 70 kPa, partial particle crushing occurs, generating finer fragments that fill the voids. This leads to a denser skeletal structure, and the positive correlation between σ_4 and Mr, σ_3 and Mr become more pronounced. Figure 6e manifests that when the CSAFR is low, insufficient hydration occurs, leading to localized enrichment of oxides on aggregate surfaces. This prevents the formation of a continuous cementitious layer, impeding interparticle contact friction and reducing material stiffness. Consequently, the M_r decreases as CSAFR increases. However, when CSAFR reaches approximately 0.2%, the quantity and quality of hydration products improve significantly, forming a dense cementitious–aggregate structure. This enhances

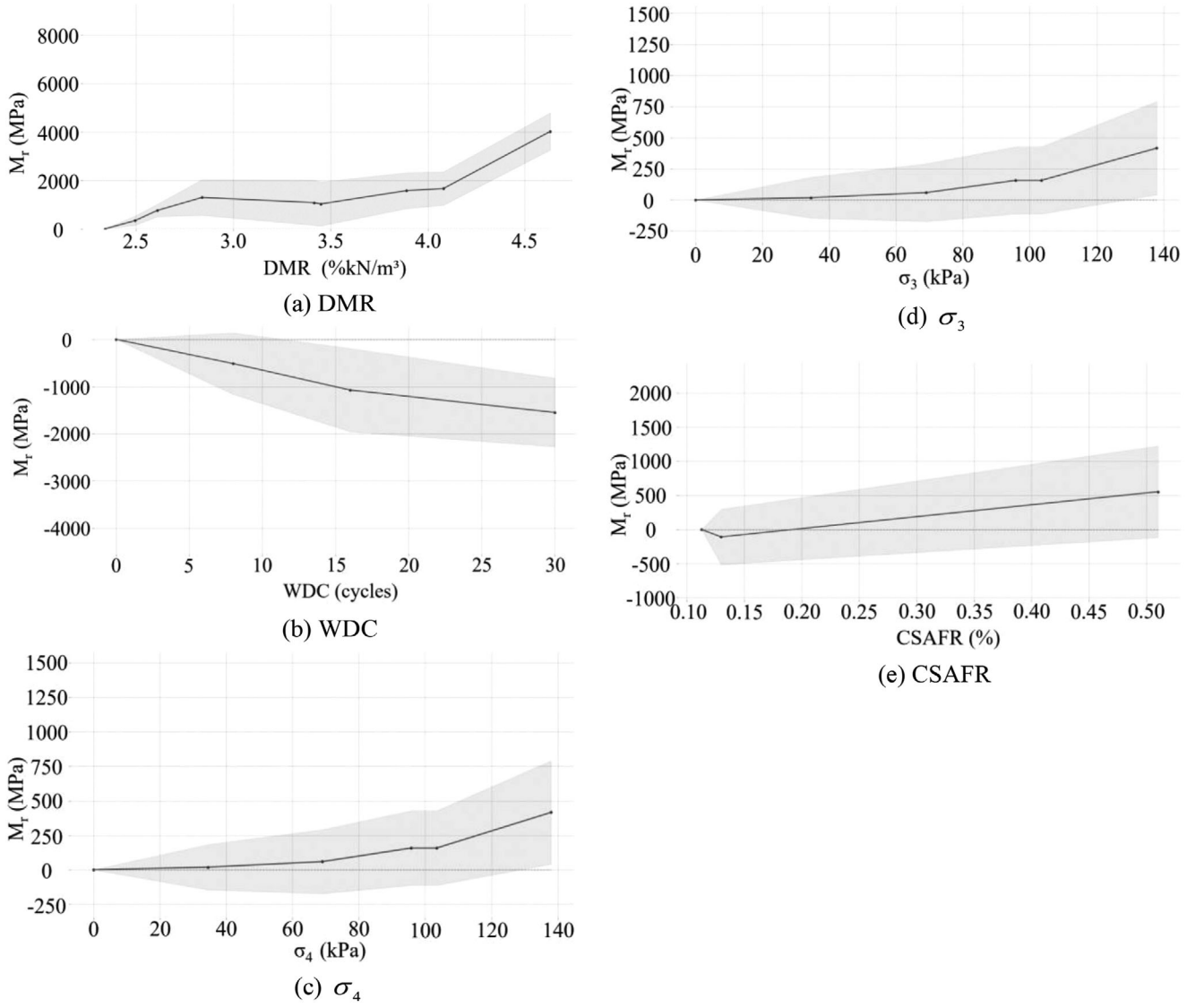

FIGURE 6 Univariate sensitivity analysis.

interparticle bonding strength and stress transfer efficiency, causing M_r to increase with further rises in CSAFR.

3.3.3 | Bivariate interaction sensitivity analysis

Bivariate interactive sensitivity analysis refers to selecting two variables from numerous uncertain factors and analyzing the degree of influence and sensitivity of these two variables on the output indicators when they change simultaneously. Its physical significance lies in uncovering the synergistic or antagonistic effects among influencing factors, thereby guiding the optimal design of stabilized aggregate base in complex environments where two factors need to be considered concurrently. As shown in Figure 7a, the increase of DMR has little impact on the positive correlation between WDC and M_r. However, when WDC is in the range of about 15 cycles to 21 cycles and 2 cycles to 6 cycles, with the increase of DMR, M_r exhibits a dynamic pattern characterized by an initial rise, a decline ensued after the increase, and then a subsequent resurgence, which is inconsistent with the trend of the M_r increasing with the increase of DMR when considering the single influence factor of DMR. The reasons for the cause of this phenomenon are likely that WDC significantly alter the microstructural and hydro-mechanical interactions within stabilized aggregate bases, thereby affecting the relationship between the DMR and the M_r. It indicates that the interaction between WDC and DMR affects the impact of DMR on the M_r when only considering DMR as a single influencing factor. Figure 7b shows the interaction influence rule of DMR and σ_4 on the M_r. The change of DMR has little influence on the positive correlation between σ_4

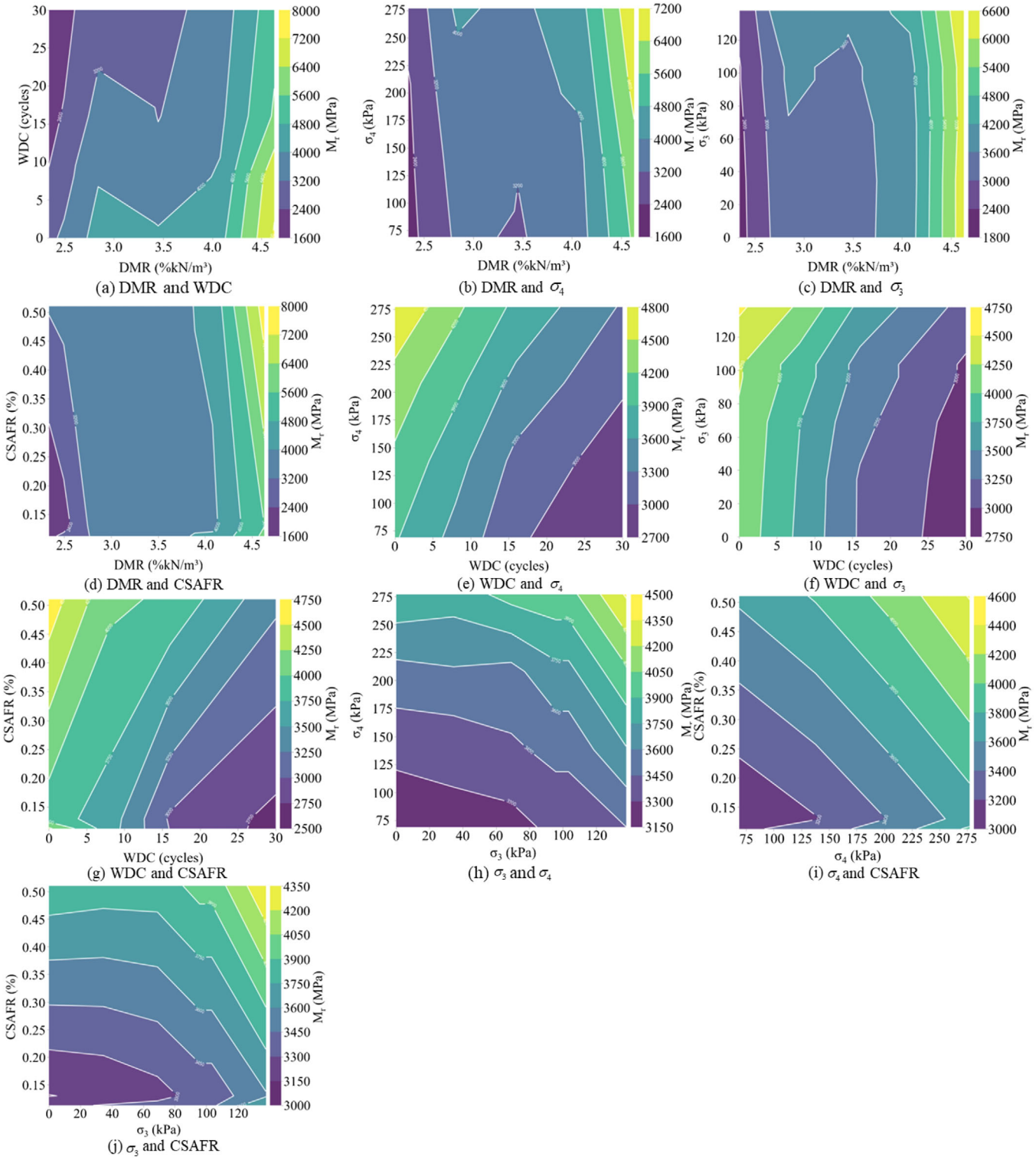

FIGURE 7 Bivariate interaction sensitivity analysis.

and M_r. When σ_4 is more than about 125 kPa and less than 250 kPa, the change of σ_4 has no influence on the positive correlation between DMR and M_r. However, when σ_4 is more than about 250 kPa or less than about 125 kPa, M_r increases first, subsequently undergoes a decline, followed by a resurgence as the DMR increases.But the abnormal state is very slight. Figure 7c shows the interaction influence rule of DMR and σ_3 on the Mr. This influence pattern is quite similar to that of the interaction influence rule of DMR and σ_4 on the M_r. DMR is essentially determined by the forming state of materials, and since σ_4 and σ_3 represent external forces, DMR will generally not affect the

relationship between σ_4 and M_r, σ_3 and M_r. Figure 7d presents the results of the interaction between DMR and CSAFR on the Mr. When DMR is less than approximately 2.7%kN/m^3 or greater than 3.7%kN/m^3, there is a slight increasing trend in the M_r with the increase in CSAFR. However, when DMR falls within the range of approximately 2.7 to 3.7 kN/m^3, the correlation between CSAFR and M_r disappears. This state likely arises due to the interaction between DMR and CSAFR, which affects the correlation between CSAFR and M_r. The sensitivity relationship between DMR and M_r appears to be unaffected by the interaction between DMR and CSAFR. Figure 7e–h depicts the sensitivity relationships of M_r to the interactions between WDC and σ_4, WDC and σ_3, WDC and CSAFR, σ_3 and σ_4, respectively. It can be observed from the figures that the interactions between them have little impact on their individual sensitivity relationships with M_r. Figure 7i,j shows the interaction sensitivity relationship of σ_4 and CSAFR, σ_3 and CSAFR to M_r. Since the sensitivity curves of M_r to σ_4 and σ_3 are relatively similar, the interaction influence rules of σ_4 and CSAFR, σ_3 and CSAFR on M_r also show a high consistency. With the change of CSAFR, the positive correlation between σ_4 and σ_3 on M_r basically does not change. With the change of σ_4 and σ_3, the sensitivity relationship between CSAFR and M_r shows an abnormal point at about 0.2%. The above analysis proves that the interaction between σ_4 and CSAFR, σ_3 and CSAFR basically does not affect the single sensitivity relationship between them and M_r.

4 | CONCLUSION

In practical applications, the M_r of stabilized aggregate base is often affected by many influencing factors, and there may be complex interaction between these factors. Sensitivity analysis of the interaction among variables that affect the M_r in stabilized aggregate bases can reveal how these variables work together to influence M_r by considering changes in multiple variables simultaneously. This analytical process facilitates a more profound comprehension of the complexity and dynamics of the M_r in stabilized aggregate bases. To elucidate the impact patterns of interactive effects among influential factors on the M_r of stabilized aggregate base, this study first established a regression prediction model for the M_r of stabilized aggregate base using the machine learning and improved the prediction accuracy of the models through hyperparameter tuning. Then, based on the model with high prediction accuracy, the importance analysis, single sensitivity analysis and bivariate interaction sensitivity analysis were analyzed. The primary findings of this investigation are encapsulated as follows.

1. Prediction models for the M_r of stabilized aggregate base were developed leveraging RF and GB. Additionally, the accuracy of these models was evaluated using cross-validation. The results of cross-validation show that GB has better performance in predicting the M_r than RF. The R^2 of the cross-validation of GB are greater than 0.97, while that of RF are only around 0.91.
2. To improve the predictive accuracy of RF and GB for M_r, hyperparameter optimization was performed using the grid search algorithm. Both RF and GB optimized by grid search algorithm led to a substantial enhancement in the precision of the predictions for the M_r of stabilized aggregate bases. The R^2 for GB in the training set and test set are 0.99 and 0.96, while the R^2 for RF in the training set and test set are 0.98 and 0.94, respectively. Compared to the two models, GB has an elevated level of predictive accuracy for the M_r of the stabilized aggregate base.
3. Based on the GB demonstrating superior predictive performance for M_r, a framework integrating SHAP for feature importance analysis and PDP for sensitivity assessment was constructed. The importance analysis indicated that DMR is the most significant indicator for the M_r, with a much greater importance than the other four influencing factors. CSAFR has the least importance for the M_r. DMR, σ_4, and σ_3 all have demonstrated a notably discernible positive association with the M_r, and the degree of influence of DMR on the M_r is about eight times greater than that of σ_4 and σ_3. As WDC increases, M_r shows a decreasing trend, and the sensitivity curve between them is close to a smooth curve, indicating that M_r decreases regularly with the increase of WDC. As CSAFR increases, M_r exhibits a phenomenon of first decreasing and then increasing.
4. Based on the pre-trained GB and PDP, a research framework was established to investigate the interaction effects among influential factors on M_r. PDP was used to realize the bivariate interaction sensitivity analysis of the influential factors. The bivariate interaction sensitivity analysis indicates that under the pairwise interactive effects of the four influencing factors, namely, WDC, σ_4, σ_3, and CSAFR, the sensitivity relationship between each single factor and M_r is basically not disrupted. However, changes in WDC have a certain disruptive effect on the sensitivity relationship between DMR and Mr. The changes in σ_4 and σ_3 also have a certain disruptive effect on the negative correlation between DMR and M_r, and the destructive patterns are similar and both very small.

This research provides an approach to understanding the relationships between different affecting variables and the M_r of stabilized aggregate base, enabling a more effective hybrid design process for more durable road infrastructure. However, this study only considered five influencing factors, which is relatively limited in scope. Moreover, it could only analyze the sensitivity of single variables and the interactive effects of bivariate interactions, without the capability to explore the influence patterns of interactions among a larger number of variables. It is recommended that future studies should include publicly available datasets collected from different geographical regions to validate, evaluate, and expand the universality of the model. Researchers can also integrate mechanical models (such as finite element simulations) with machine learning models to enhance the interpretability and physical consistency of the models. Additionally, they can consider incorporating more factors, including gradation, curing age, and dynamic load frequency, to analyze the influence patterns of a broader range of factors on the M_r of stabilized aggregate base.

REFERENCES

Alzubi, M. A., Ahmad, M., Abdullah, S., Khan, B. J., Qamar, W., Abdullah, G. M. S., González-Lezcano, R. A., Paul, S., El-Gawaad, N. S. A., & Ouahbi, T. (2024). Long short term memory networks for predicting resilient modulus of stabilized base material subject to wet-dry cycles. *Scientific Reports*, *14*(1), 27928. https://doi.org/10.1038/s41598-024-79588-5

Arulrajah, A., Perera, S., Wong, Y. C., Maghool, F., & Horpibulsuk, S. (2021). Stabilization of pet plastic-demolition waste blends using fly ash and slag-based geopolymers in light traffic road bases/subbases. *Construction and Building Materials*, *284*, 122809. https://doi.org/10.1016/j.conbuildmat.2021.122809

Berangi, M., Lontra, B. M., Anupam, K., Erkens, S., Van Vliet, D., Snippe, A., & Moenielal, M. (2025). Gradient boosting decision trees to study laboratory and field performance in pavement management. *Computer-Aided Civil and Infrastructure Engineering*, *40*(1), 3–32. https://doi.org/10.1111/mice.13322

Bui, K.-T. T., Torres, J. F., Gutierrez-Aviles, D., Nhu, V.-H., Bui, D. T., & Martinez-Alvarez, F. (2022). Deformation forecasting of a hydropower dam by hybridizing a long short-term memory deep learning network with the coronavirus optimization algorithm. *Computer-Aided Civil and Infrastructure Engineering*, *37*(11), 1368–1386. https://doi.org/10.1111/mice.12810

Chowdhury, S. M. R. M. (2021). Evaluation of resilient modulus constitutive equations for unbound coarse materials. *Construction and Building Materials*, *296*(7), 123688. https://doi.org/10.1016/j.conbuildmat.2021.123688

Fan, A., Wang, Y., Yang, L., Yang, Z., & Hu, Z. (2025). A novel grey box model for ship fuel consumption prediction adapted to complex navigating conditions. *Energy*, *315*, 134436. https://doi.org/10.1016/j.energy.2025.134436

Fernandes Filho, C. C., Andrade, M. H. M. L., Nunes, J. A. R., Jarquin, D. H., & Rios, E. F. (2023). Genomic prediction for complex traits across multiples harvests in alfalfa (*Medicago Sativa L.*) is enhanced by enviromics. *Plant Genome*, *16*(2), e20306.

Ghanizadeh, A. R., & Rahrovan, M. (2016). Application of artifitial neural network to predict the resilient modulus of stabilized base subjected to wet dry cycles. *Computations and Materials in Civil Engineering*, *1*, 37–47.

Heidarabadizadeh, N., Ghanizadeh, A. R., & Behnood, A. (2021). Prediction of the resilient modulus of non-cohesive subgrade soils and unbound subbase materials using a hybrid support vector machine method and colliding bodies optimization algorithm. *Construction and Building Materials*, *275*, 122140. https://doi.org/10.1016/j.conbuildmat.2020.122140

Hu, Q. S., Zhang, J. P., He, Y. Z., Li, J. B., Song, C. Y., & Li, G. C. (2023). Investigation of mechanical properties, stiffness, and flexibility of cold recycled cement-stabilized gravel base milling mixes with foamed asphalt. *Journal of Materials in Civil Engineering*, *35*(12). https://doi.org/10.1061/JMCEE7.MTENG-16208

Huang, J. D., Zhou, M. M., Zhang, J., Ren, J. L., Vatin, N. I., & Sabri, M. M. S. (2022). Development of a new stacking model to evaluate the strength parameters of concrete samples in laboratory. *Iranian Journal of Science and Technology-Transactions of Civil Engineering*, *46*(6), 4355–4370. https://doi.org/10.1007/s40996-022-00912-y

Huang, R., Zhang, X., & Liu, K. (2024). Assessment of operational carbon emissions for residential buildings comparing different machine learning approaches: A study of 34 cities in China. *Building and Environment*, *250*, 111176. https://doi.org/10.1016/j.buildenv.2024.111176

Huang, Y. M., Huo, Z. H., Ma, G. W., Zhang, L., Wang, F., & Zhang, J. F. (2023). Multi-objective optimization of fly ash-slag based geopolymer considering strength, cost and CO_2 emission: A new framework based on tree-based ensemble models and NSGA-II. *Journal of Building Engineering*, *68*, 106070. https://doi.org/10.1016/j.jobe.2023.106070

Ikeagwuani, C. C., & Nwonu, D. C. (2022). Statistical analysis and prediction of spatial resilient modulus of coarse-grained soils for pavement subbase and base layers using MLR, ANN and ensemble techniques. *Innovative Infrastructure Solutions*, *7*(4), 19. https://doi.org/10.1007/s41062-022-00875-z

Ikeagwuani, C. C., Nwonu, D. C., & Nweke, C. C. (2022). Resilient modulus descriptive analysis and estimation for fine-grained soils using multivariate and machine learning methods. *International Journal of Pavement Engineering*, *23*(10), 3409–3424. https://doi.org/10.1080/10298436.2021.1895993

Jahanshahi, F. S., & Ghanizadeh, A. R. (2025). Machine learning approaches for resilient modulus modeling of cement-stabilized magnetite and hematite iron ore tailings. *Scientific Reports*, *15*(1), 4950.

Jeong, J., Jeong, J., Lee, M., Lee, J., & Chang, S. (2022). Data-driven approach to develop prediction model for outdoor thermal comfort using optimized tree-type algorithms. *Building and Environment*, *226*, 109663. https://doi.org/10.1016/j.buildenv.2022.109663

Kaloop, M. R., Kumar, D., Samui, P., Gabr, A. R., Hu, J. W., Jin, X., & Roy, B. (2019). Particle swarm optimization algorithm-extreme learning machine (PSO-ELM) model for predicting resilient modulus of stabilized aggregate bases. *Applied Sciences-Basel*, *9*(16), 3221.

Kamran, F., Basavarajappa, M., Bala, N., & Hashemian, L. (2021). Laboratory evaluation of stabilized base course using asphalt emulsion and asphaltenes derived from Alberta oil sands. *Construction and Building Materials*, *283*, 122735. https://doi.org/10.1016/j.conbuildmat.2021.122735

Khan, A., Huyan, J., Zhang, R., Zhu, Y., Zhang, W., Ying, G., Ahmad, K. N., & Shah, S. K. (2023). An ensemble tree-based prediction of marshall mix design parameters and resilient modulus in stabilized base materials. *Construction and Building Materials*, *401*, 132833. https://doi.org/10.1016/j.conbuildmat.2023.132833

Khan, K., Jalal, F. E., Khan, M. A., Salami, B. A., Amin, M. N., & Alabdullah, A. A., Samiullah, Q., Abu Arab, A. M., Faraz, M. I., & Iqbal, M. (2022). Prediction models for evaluating resilient modulus of stabilized aggregate bases in wet and dry alternating environments: ANN and GEP approaches. *Materials*, *15*(13), 4386. https://doi.org/10.3390/ma15134386

Khattak, A., Chan, P.-W., Chen, F., & Peng, H. (2023). Estimating turbulence intensity along the glide path using wind tunnel experiments combined with interpretable tree-based machine learning algorithms. *Building and Environment*, *239*, 110385. https://doi.org/10.1016/j.buildenv.2023.110385

Khoury, N., & Zaman, M. M. (2007). Durability of stabilized base courses subjected to wet–dry cycles. *International Journal of Pavement Engineering*, *8*(4), 265–276. https://doi.org/10.1080/10298430701342874

Kim, S.-H., Yang, J., & Jeong, J.-H. (2014). Prediction of subgrade resilient modulus using artificial neural network. *KSCE Journal of Civil Engineering*, *18*(5), 1372–1379. https://doi.org/10.1007/s12205-014-0316-6

Liang, M., Chang, Z., He, S., Chen, Y., Gan, Y., Schlangen, E., & Savija, B. (2022). Predicting early-age stress evolution in restrained concrete by thermo-chemo-mechanical model and active ensemble learning. *Computer-Aided Civil and Infrastructure Engineering*, *37*(14), 1809–1833. https://doi.org/10.1111/mice.12915

Liu, K., Dai, Z., Zhang, R., Zheng, J., Zhu, J., & Yang, X. (2022). Prediction of the sulfate resistance for recycled aggregate concrete based on ensemble learning algorithms. *Construction and Building Materials*, *317*, 125917. https://doi.org/10.1016/j.conbuildmat.2021.125917

Liu, P., Du, C., Friederichs, J., Wang, Y., Hu, J., & Leischner, S. (2023). Multiscale modelling and simulation for asphalt pavements under moving tire footprint loads. *International Journal of Pavement Engineering*, *24*(1), 2154349. https://doi.org/10.1080/10298436.2022.2154349

Liu, Y., Yu, Y., Ouyang, J., Jiang, B., Ostmeier, S., Wang, J., Lu-Liang, S., Yang, Y., Yang, G., Michel, P., Liebeskind, D. S., Lansberg, M., Moseley, M. E., Heit, J. J., Wintermark, M., Albers, G., & Zaharchuk, G. (2024). Prediction of ischemic stroke functional outcomes from acute-phase noncontrast CT and clinical information. *Radiology*, *313*(1),. https://doi.org/10.1148/radiol.240137

Maalouf, M., Khoury, N., Laguros, J. G., & Kumin, H. (2012). Support Vector regression to predict the performance of stabilized aggregate bases subject to wet-dry cycles. *International Journal for Numerical and Analytical Methods in Geomechanics*, *36*(6), 675–696. https://doi.org/10.1002/nag.1023

Mathew, T., Johnpaul, C. I., Ajith, B., Kini, J. R., & Rajan, J. (2023). A deep learning based classifier framework for automated nuclear atypia scoring of breast carcinoma. *Engineering Applications of Artificial Intelligence*, *120*, 105949. https://doi.org/10.1016/j.engappai.2023.105949

Mizher, D., Tsang, H. H., & Disfani, M. M. (2024). Effects of bitumen on shear strength parameters of soil-rubber mixtures. *Case Studies in Construction Materials*, *20*, e03094. https://doi.org/10.1016/j.cscm.2024.e03094

Qi, C. C., Wu, M. T., Zheng, J. S., Chen, Q. S., & Chai, L. Y. (2022). Rapid identification of reactivity for the efficient recycling of coal fly ash: Hybrid machine learning modeling and interpretation. *Journal of Cleaner Production*, *343*, 130958. https://doi.org/10.1016/j.jclepro.2022.130958

Rafie, A., el Berrouhi, S., Chenouni, D., Tahiri, A., & el Mallahi, M. (2023). AI-based feature parameters extraction from color images. *Multimedia Tools and Applications*, *83*, 51715–51729. https://doi.org/10.1007/s11042-023-17193-w

Ribeiro, V. H. A., Santana, R., & Reynoso-Meza, G. (2023). Random vector functional link forests and extreme learning forests applied to UAV automatic target recognition. *Engineering Applications of Artificial Intelligence*, *117*, 105538.

Rust, F. C., Smit, M. A., Akhalwaya, I., Jordaan, G. J., & du Plessis, L. (2022). Evaluation of two nano-silane-modified emulsion stabilised pavements using accelerated pavement testing. *International Journal of Pavement Engineering*, *23*(5), 1339–1352. https://doi.org/10.1080/10298436.2020.1799210

Shah, A., Thaker, T., Shukla, V., & Ranpura, P. (2024). Efficient predictive modeling of resilient modulus in stabilized clayey soil using automated machine learning. *Construction and Building Materials*, *442*, 137678. https://doi.org/10.1016/j.conbuildmat.2024.137678

Sharma, R. K., Singh, D., & Dasaka, S. M. (2024). Investigating supplementary cementitious materials' effects on stabilized aggregate performance, behaviour, and design aspects. *Construction and Building Materials*, *411*, 134564. https://doi.org/10.1016/j.conbuildmat.2023.134564

Swarna, S. T., & Hossain, K. (2023). Asphalt binder selection for future canadian climatic conditions using various pavement temperature prediction models. *Road Materials and Pavement Design*, *24*(2), 447–461. https://doi.org/10.1080/14680629.2021.2019093

Wang, Y., Chen, J., Hu, Y., & Weng, X. (2023). Modelling and interpreting evacuation time and exit choice for large-scale ancient architectural complex using machine learning. *Journal of Building Engineering*, *80*, 108133. https://doi.org/10.1016/j.jobe.2023.108133

Wilde, W. J., Tutumluer, E., Xiao, Y. J., Beaudry, T., & Siekmeier, J. (2016). Optimizing stability and stiffness through aggregate base gradation. *Transportation Research Record*, 12–20. https://doi.org/10.3141/2578-02

Wu, M. T., Qi, C. C., Chen, Q. S., & Liu, H. (2023). Evaluating the metal recovery potential of coal fly ash based on sequential extraction and machine learning. *Environmental Research*, *224*, 115546. https://doi.org/10.1016/j.envres.2023.115546

Xiao, Y., Jin, M., Qi, G., Shi, W., Li, K. X., & Du, X. (2024). Interpreting the influential factors in ship detention using a novel random forest algorithm considering dataset imbalance and uncertainty. *Engineering Applications of Artificial Intelligence*, *133*, 108369. https://doi.org/10.1016/j.engappai.2024.108369

Yu, X., Lu, S., Guo, L., Wang, S. H., & Zhang, Y. D. (2021). ResGNet-C: A graph convolutional neural network for detection of COVID-19.

Neurocomputing, *452*, 592–605. https://doi.org/10.1016/j.neucom.2020.07.144

Zhang, H., Tan, J., Zhang, J., Chen, Y., & Jing, L. (2022). Double information preserving canonical correlation analysis. *Engineering Applications of Artificial Intelligence*, *112*, 104870. https://doi.org/10.1016/j.engappai.2022.104870

Zhang, J. F., Xu, C. H., Zhang, L., & Wang, L. (2025). Intelligent design of mixture proportions of manufactured sand concrete from environmental, economical and mechanical perspectives. *Case Studies in Construction Materials*, *22*, e04637.

Zhang, X., Yan, K., & Liu, W. (2023). Partially replacing cement with rice husk ash (RHA) in cement stabilised macadam (CSM) containing reclaimed asphalt pavement (RAP) for qualified base materials. *Road Materials and Pavement Design*, *24*(10), 2483–2503. https://doi.org/10.1080/14680629.2022.2150275

Zhao, P. X., Li, K. C., Zhou, N. N., Chen, Q. S., Zhou, M., & Qi, C. C. (2025). Enhanced prediction of occurrence forms of heavy metals in tailings: A systematic comparison of machine learning methods and model integration. *International Journal of Minerals Metallurgy and Materials*, Advanced online publication. https://doi.org/10.1007/s12613-025-3136-4

Zhu, S., Yan, Y., Zhao, B., & Wang, H. (2025). Assessing the impact of adjacent urban morphology on street temperature: A multi-source analysis using random forest and SHAP. *Building and Environment*, *267*, 112326. https://doi.org/10.1016/j.buildenv.2024.112326

How to cite this article: Guo, M., Zhou, M., Du, X., & Liu, P. (2025). Machine learning-based analysis of interaction effects among influencing factors on the resilient modulus of stabilized aggregate base. *Computer-Aided Civil and Infrastructure Engineering*, 1–16. https://doi.org/10.1111/mice.70102